Preliminary Study of the Combined Function Magnets used in the 20-GeV Feasibility II Muon Storage Ring

K. Makino

The study was supported by
C.J. Johnstone (Fermilab),
M. Berz and B. Erdelyi (Michigan State University), and
D. Errede (University of Illinois at Urbana-Champaign)

Abstract

In the design of a compact 20-GeV muon storage ring for the Feasibility II Study of a Neutrino Factory, combined-function, skew-quadrupole magnets have been introduced which represent a completely new magnet design. These magnets are not even approximately represented in current "state of the art" optics codes. Hence a study has been undertaken to formulate simple, 2D models for these magnets and obtain a preliminary multipole decomposition. The impact of the allowed multipoles and their strengths are then studied by tracking techniques. This paper reports the methodologies used and a comparison of magnet models along with the results from tracking the storage ring arcs using the code, COSY Infinity [1]. Since a 2D model does not correctly describe the strong longitudinal dependencies of these multipoles, a 3D extension of one approach was undertaken as an initial exploration into a full simulation.

1 Introduction

Location of a muon storage ring for a Neutrino Factory on the Brookhaven National Laboratory site requires a high degree of compactness of the arcs in order to optimize the proportion of decay straight to total circumference, which maximizes the usable neutrinos produced. To this end, new superconducting coil configurations have been proposed [2]: In effect coils offset longitudinally from one another as shown in Figure 1. In the region with a coil both top and bottom, one has a, more or less, standard dipole. The regions with only a single coil, the effect is that of a dipole plus an alternating-gradient, skew quadrupole field. Dipole and quadrupole gradients are carefully adjusted in

both planes to preserve cylindrically-symmetric focusing, which has the effect of eliminating coupling in the linear optics.

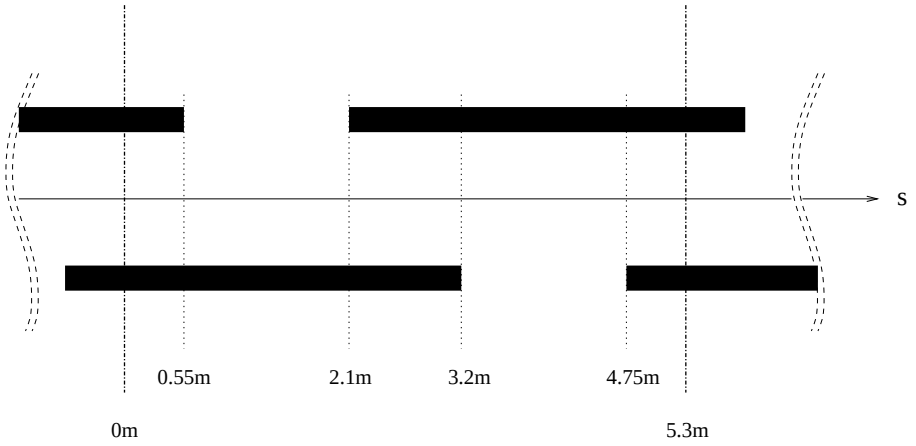

Fig. 1. Longitudinal coil configuration.

However, because of the coupling the performance of the entire ring, not only its dynamic aperture, is strongly dependent on the type and strength of nonlinearities. Fringe fields which are relatively benign in a correctly-designed upright ring with midplane symmetry break the decoupling in this ring resulting in strong, high-order dependencies apparent in the particle trajectories. Further, one does not have the experience on which to base assumptions of achievable field quality as one has with conventional magnets – in particular there is no experience with the important skew multipoles from a single coil and its end fields. Perhaps even more important is the breaking of midplane symmetry which occurs in the entire single coil region along the x direction and at the transition region between the double coil and the single coil along the s direction. For example, without correction, there is no central orbit relative to the magnet poles because of the break in midplane symmetry. The particle at the center of the magnets undergoes a kick when traversing the region between the two coils and the single coil.

There are quite a number of issues which must be confronted in order to adequately simulate this completely new magnet design and coupled ring optics. This report discusses two approaches to developing a model of the lattice from which the allowed multipoles can be derived and their strengths estimated. The two models serve as a cross check and provide initial results for the dynamic aperture and very preliminary limiting values for the strengths of the multipoles – but only for the 2D case. Subsequent to the 2D study, an s-dependence of the field was extracted analytically from the bar-magnet model [3,4]. Because of the absence of midplane symmetry, a longitudinal magnetic field arises between the displaced coils, creating a net solenoidal field with associated spherical lens focusing and nonlinearities; the strength of the longitudinal component depends not only on the magnitude of the central field, but also on the extent of longitudinal displacement and on the trans-

verse magnet aperture. (For two non-overlapping coils, the field between them becomes completely longitudinal as their transverse separation goes to zero.) The calculated s-dependent field profile is then superimposed onto the "optimized" 2D simulation to create an approximate 3D representation. The results of this study will be reported also.

2 Description of Approaches and Models

In the study reported here, only the 60° arc cell is simulated, as the matching and production regions represent studies of a different nature.

For the purposes of verifying the simulations, two sets of multipole decompositions have been used, both of them employing 2D data only. The first is based on 2D field simulations performed by Ramesh Gupta at BNL with the codes Poisson, Opera 2D and other codes. The other is based on the analytically known field of a uniformly magnetized rectangular surface of infinite depth [3,4] representing the two pole surfaces in the overlapping double coil case and the single pole surface in the case of the single coil that is the dipole with superimposed skew quadrupole.

When using identical geometric data for the double coil region magnets based on the preliminary design provided by R. Gupta at BNL (on Feb. 7, 8th in 2001), the normal and skew multipole decompositions obtained for the 2D case are similar, which gives support to both of the 2D multipole data. Figure 2 shows the magnet geometry for each case and Table 1 shows the magnitudes of the multipoles relative to the dipole component, normalized to their magnitude at 2cm US convention reference radius for ease of comparison. There is no skew component in this case.

Table 1
For comparison purposes, the two sets of 2D multipole decompositions for the infinitely long double coil region. The data is at 2cm US convention reference radius.

		2D coil model by Gupta	3D bar magnet model
0	Dipole	1	1
2	Sextupole	-1.07E-2	-5.644778029413420E-3
4	Decapole	-4.60E-4	-6.115840716166541E-5
6	14-pole	-6.435E-6	-3.531242002451424E-7
8	18-pole	1.966E-5	2.880573657687675E-9
10	22-pole	6.015E-7	1.096571701274581E-10
12	26-pole	-6.887E-6	1.438831464833482E-12

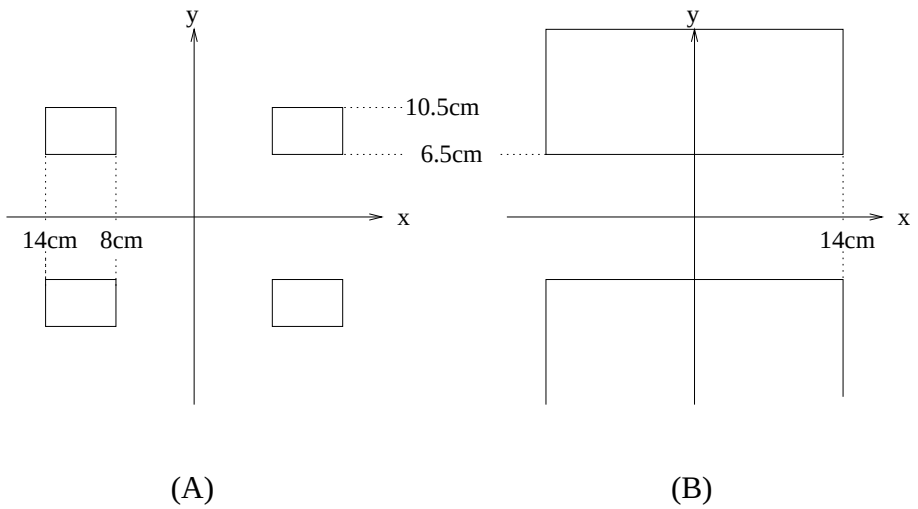

Fig. 2. Magnet geometry. (A) is the 2D coil configuration used by R. Gupta. (B) is the 3D placement of the two rectangular bar magnets which extend infinitely in the z direction.

The bar magnet approach can be used to estimate the multipole components when the magnets are placed to emulate the arc cell design. Four bar magnets with longitudinal length 3.75m are placed like in Figure 1, and the resulting multipole decompositions are listed in Table 2 (B). The maximum dipole strength at the center of the double coil region is assumed to be 7T, and all the components are scaled to the field strength at the pole tip of 6.5cm, so that they can be used right away in the simulation with COSY Infinity [1] using elements that can handle normal and skew multipole components simultaneously.

This set of data on multipole components gives a good insight into the correlation between the double coil region and the single coil region. As noted above, there is no skew component in the double coil region. The normal components in the single coil region are about a half of those of the double coil region and there are skew components as well. The skew components change the sign if the single coil is at the lower position instead of the upper position.

Listed also in Table 2 (A) is a set of multipole components based on the data supplied by R. Gupta (on Feb. 7, 8th). The maximum dipole strength at the center of the double coil region is set to be 6.35T as supplied, and all the components are scaled in the same way to the bar magnet model case. The supplied data is limited to the 2D case, so the correlation we learned from the bar magnet model was applied to set up a full set of multipole components.

We take the dipole and the quadrupole components as they were included in the 60° arc cell lattice listed in Table 3, and we only add the multipole components higher and equal to that of the sextupole. In the following computation, the set of multipole components based on Gupta's data is used.

Table 2
Multipole decompositions. (A) is based on the data supplied by R. Gupta, and is used for the simulation. (B) is calculated using four bar magnets arraigned longitudinally (See Figure 1). Both are scaled to the field strength at the pole tip 6.5cm radius.

(A) Multipole Decompositions based on Gupta's Data				
		Double Coil Region	Single Coil Region (b)	
		Normal Components	Normal Components	Skew Components
0	Dipole	6.35	—	0
1	Quadrupole	0	0	—
2	Sextupole	-0.721874127471	-0.360937063736	0
3	Octupole	0	0	0.100208577080
4	Decapole	-0.325677875510	-0.162838937755	0
5	Duodecapole	0	0	0.105845309541
6	14-pole	-0.481545275671E-1	-0.240772637835E-1	0
7	16-pole	0	0	-0.111799108203

(B) Multipole Decompositions for Four Bar Magnets				
		Double Coil Region	Single Coil Region (b)	
		Normal Components	Normal Components	Skew Components
0	Dipole	7.0	3.540958193499	0
1	Quadrupole	0	0	1.184123248558
2	Sextupole	-0.419967202357	-0.209972229705	0
3	Octupole	0	0	0.203438043890E-1
4	Decapole	-0.480588041860E-1	-0.240293996980E-1	0
5	Duodecapole	0	0	-0.465339592000E-2
6	14-pole	-0.293096719400E-2	-0.146548359800E-2	0
7	16-pole	0	0	-0.103494532800E-2
8	18-pole	0.252539422000E-3	0.126269711000E-3	0
9	20-pole	0	0	-0.102938909000E-3
10	22-pole	0.101543927000E-3	0.507719630000E-4	0
11	24-pole	0.	0	0.143462300000E-5
12	26-pole	0.140732230000E-4	0.703661100000E-5	0
13	28-pole	0	0	0.251896500000E-5

3 Results of the 2D Simulations

3.1 Translation from Thin-Lenses to Non-Zero Length Elements, and the Fringe Field Effects

For a point of reference, tracking simulations were performed assuming only a body sextupole component to correct the linear chromaticity of the arc cell. The parameters of the elements in the 60° arc cell are listed in Table 3. The magnet aperture is assumed to be $\pm 6.5cm$. A kick approach is a commonly employed, and sometimes only available method to include multipole components in conventional codes like MAD. While it is convenient to superimpose additional higher order multipole components, it cannot treat any detail of the field like fringe field effects. The inspection of the nonlinear effects in the ring designed in linear optics is the main purpose of this report, so we first translated several thin-lens model kick elements to the equivalent non-zero length elements to superimpose with negative drifts. These thin-lens elements were placed in the sections (b') and (e') in Table 3. The length of the superposition with negative drift should be reasonably short, so both the double coil 1.10m section and the single coil 1.55m section are split to ten pieces each. For the confirmation of the translation, the 60° cell is tracked to the stability limit, where the initial particles are launched in the horizontal plane at $x = 10, 20, ..., 70cm$, and the x-a motion and x-y motion are studied by tracking as shown in Figure 3. (a is the x momentum slope, p_x/p_0.) The scales of the pictures extend to $x : \pm 150cm$, $a : \pm 0.5$ and $y : \pm 100cm$. We also show the result in much smaller region for the later comparison purpose in Figure 4; the initial particles are launched at $x = 0.5, 1.0, 1.5, ..., 3.5cm$, and this setting is used in the rest of this report. In this case, the scales of the pictures extend to $x : \pm 7.5cm$, $a : \pm 0.025$ and $y : \pm 5cm$. So far, no fringe field effects are considered.

As can be seen in Figures 4, the performance of the 60° arc cells is almost completely linear in the region we are interested in as expected; the decoupling of the two planes is clearly intact. The linear stability holds well beyond this limit as seen in Figure 3. Then, to test the effect of nonlinearities, a set of standard Enge-function falloffs, prepared by default in COSY Infinity, was inserted as an end field to the double coil/single coil transition points. While this is not directly applicable to the problem at hand, it at least provides an indication of the degree of coupling which can be expected to arise from errors and fringe fields [5]. The tracking pictures in Figure 5 show clear coupling effects, with particles launched in the horizontal plane walking in a pattern through the vertical plane. This coupling has strong implications for steering and orbit correction. However, with just a normal quadrupole end field, the dynamic aperture is still robust and relatively unaffected by this type and

location of nonlinearities.

Table 3

Elements in the 60° arc cell. $k_1 = (\partial B_y/\partial x)/(B\rho)$, $k_2 = (\partial^2 B_y/\partial x^2)/(B\rho)$. $(B\rho)$ for a 20 GeV muon is 67.064332, B_D is the dipole field strength, B_Q and B_H are the quadrupole and sextupole field strength at the aperture $d = 6.5cm$.

Section	Starting Position	Length	Tilt Angle	Deflection (B_D)	k_1 (B_Q)	k_2 (B_H)
(a)	0.00m	0.55m	45°	3.30° (7.02296T)	-0.00548 (-0.02389T)	0
(b)	0.55m	1.55m	45°	4.65° (3.51148T)	-0.00137 (-0.00597T)	0
(b')			0°	0°	-0.30269 (-1.31950T)	-0.01932 (-0.002737T)
(c)	2.10m	0.55m	45°	3.30° (7.02296T)	-0.00548 (-0.02389T)	0
(d)	2.65m	0.55m	45°	3.30° (7.02296T)	-0.00548 (-0.02389T)	0
(e)	3.20m	1.55m	45°	4.65° (3.51148T)	-0.00137 (-0.00597T)	0
(e')			0°	0°	0.30269 (1.31950T)	0.01317 (0.001866T)
(f)	4.75m	0.55m	45°	3.30° (7.02296T)	-0.00548 (-0.02389T)	0

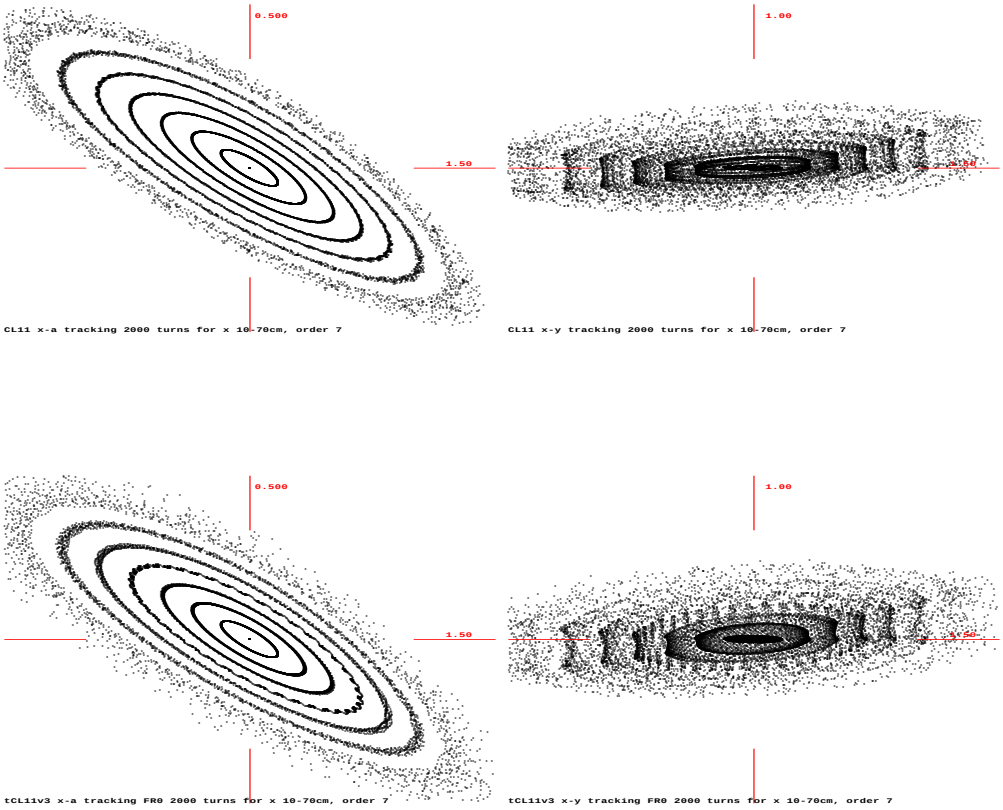

Fig. 3. Tracking particles starting at $x = 10, ..., 70cm$ in the 60° arc cell with thin-lens model elements (top two) and with the equivalent non-zero length elements (bottom two) in x-a motion (left) and x-y motion (right). The scales of the pictures extend to $x : \pm 150cm$, $a : \pm 0.5$ and $y : \pm 100cm$.

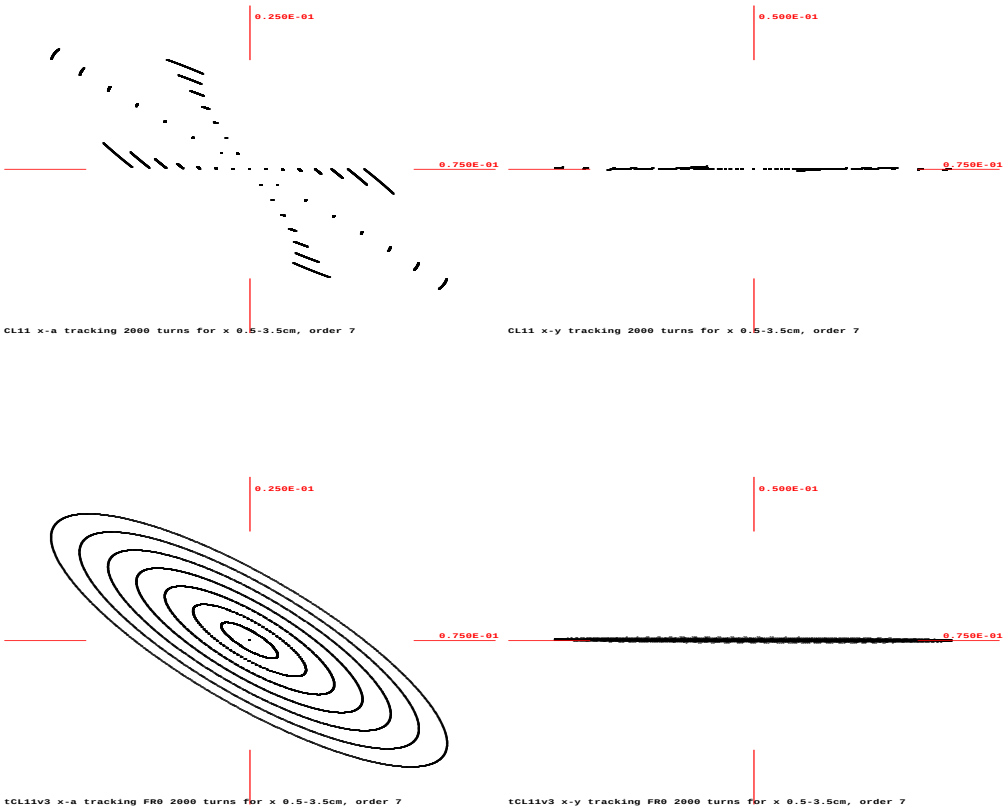

Fig. 4. Tracking particles starting at $x = 0.5, ..., 3.5cm$ with thin-lens model elements (top two) and with the equivalent non-zero length elements (bottom two) in x-a motion (left) and x-y motion (right). The scales of the pictures extend to $x : \pm 7.5cm$, $a : \pm 0.025$ and $y : \pm 5cm$.

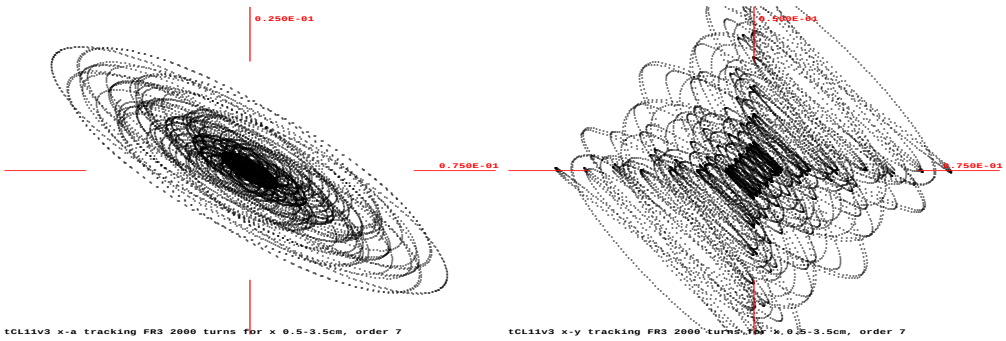

Fig. 5. Tracking particles with Enge falloff fringe fields applied to the arc cell in Table 3 and Figure 4.

3.2 Effects by Additional Multipole Components

With a robust linear design, the next step is to use the additional multipole strengths calculated from the models. As previously stated, the decompositions from the 2D magnet simulation were explicitly used, although similar results are expected from both sets. It is important to note that we expect that much more than a 2D multipole decomposition will be needed in order to assess the performance. There are extended fringe fields leading to a significant longitudinal dependence of multipoles. In the following, along with the effects by the additional main body higher multipole components, we study the fringe field effects in parallel using the standard Enge-function falloffs.

Figure 6 shows the effect of the additional large multipoles, and their impact on the dynamic aperture is catastrophic. Adding a standard fringe field represents negligible further deterioration. The initial multipole content was abnormally large with the normal sextupole, skew octupole and normal decapole terms occupying 10%, 3%, and 5% of the proposed central dipole strength of 7 T, respectively. Consequently, a study was initiated to determine at what level the offending multipoles could be tolerated and sustain an acceptable dynamic aperture. It was found that its effect began to diminish signficantly at a level 10% of the initial calculation of the body sextupole component. Further studies indicated the skew octupole and normal decapole also require an order of magnitude reduction in their strength to allow an acceptable dynamic aperture. Figures 7 through 9 show a partial restoration of the dynamic aperture using these decreased multipole strengths with and without an assumed fringe field. Table 4 lists the additional body multipole setting for each study case. The last set, where all the sextupole, octupole and decapole components are 10% of the initial data, is the recommended limiting values for these three offending multipoles, and it is adopted for the study in the next section.

Table 4
Additional multipole strength in each study case.

Figure	Normal Sextupole	Skew Octupole	Normal Decapole	Higher
6	Full as (A) in Table 2			
7	0	Full	Full	Full
8	10%	Full	Full	Full
9	10%	10%	10%	Full
11, 12, 13	10%	10%	10%	Full

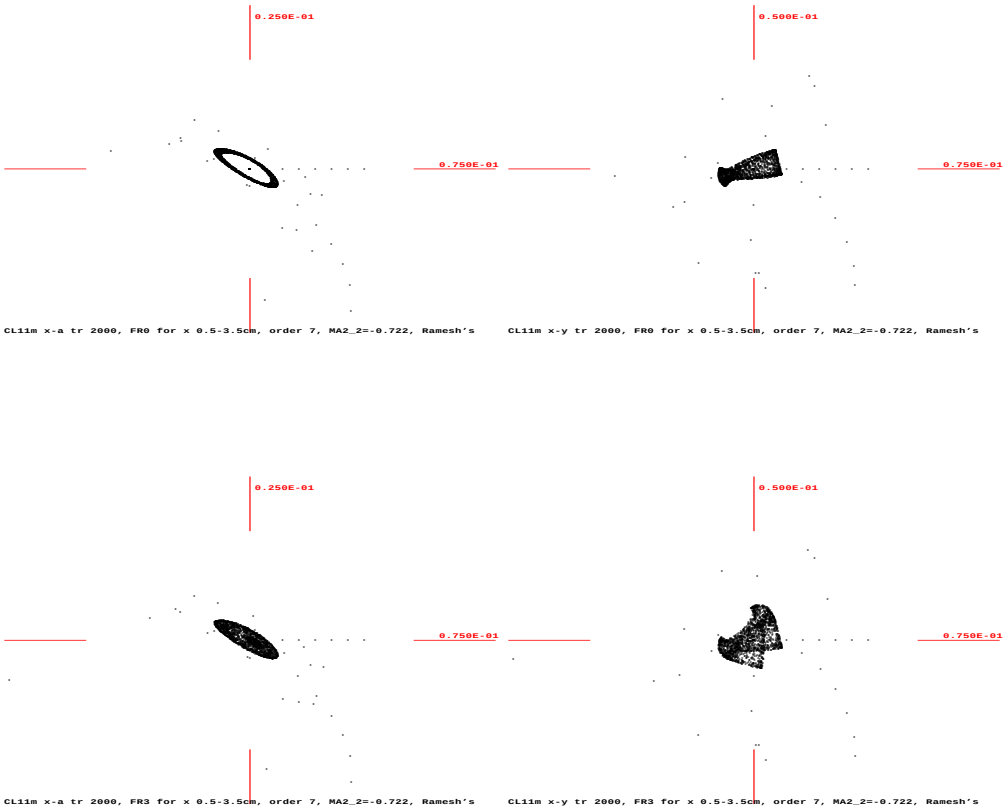

Fig. 6. Tracking the arc cell with the additional multipole components supplied by R. Gupta listed in Table 2. Without (top two) and with (bottom two) the fringe field consideration.

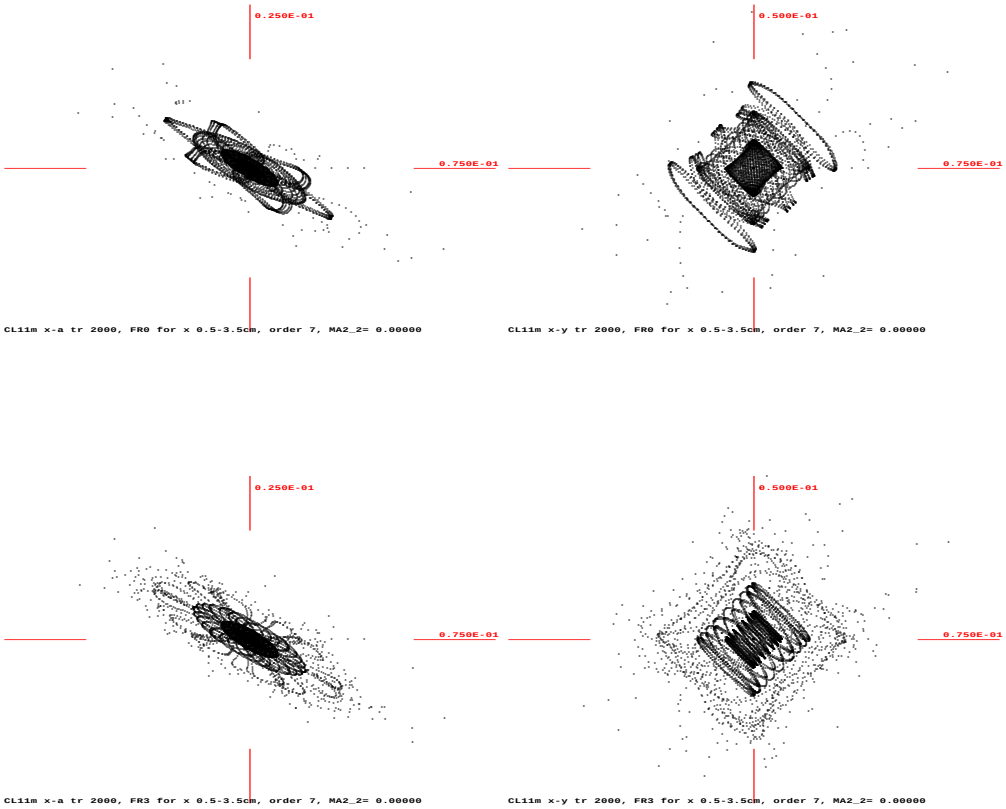

Fig. 7. Tracking with the additional multipole components but the sextupole components. Without/with (top/bottom) the fringe field consideration.

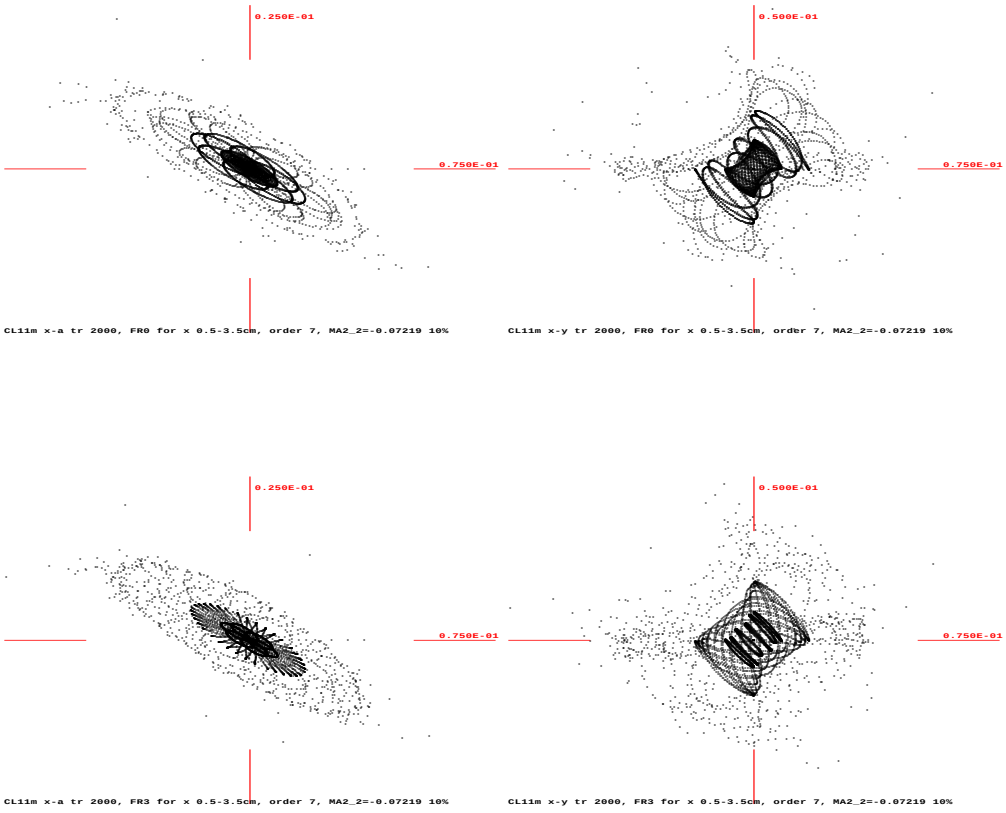

Fig. 8. Tracking with the additional multipole components, with the normal sextupole strength 10% of the initial. Without/with (top/bottom) the fringe field consideration.

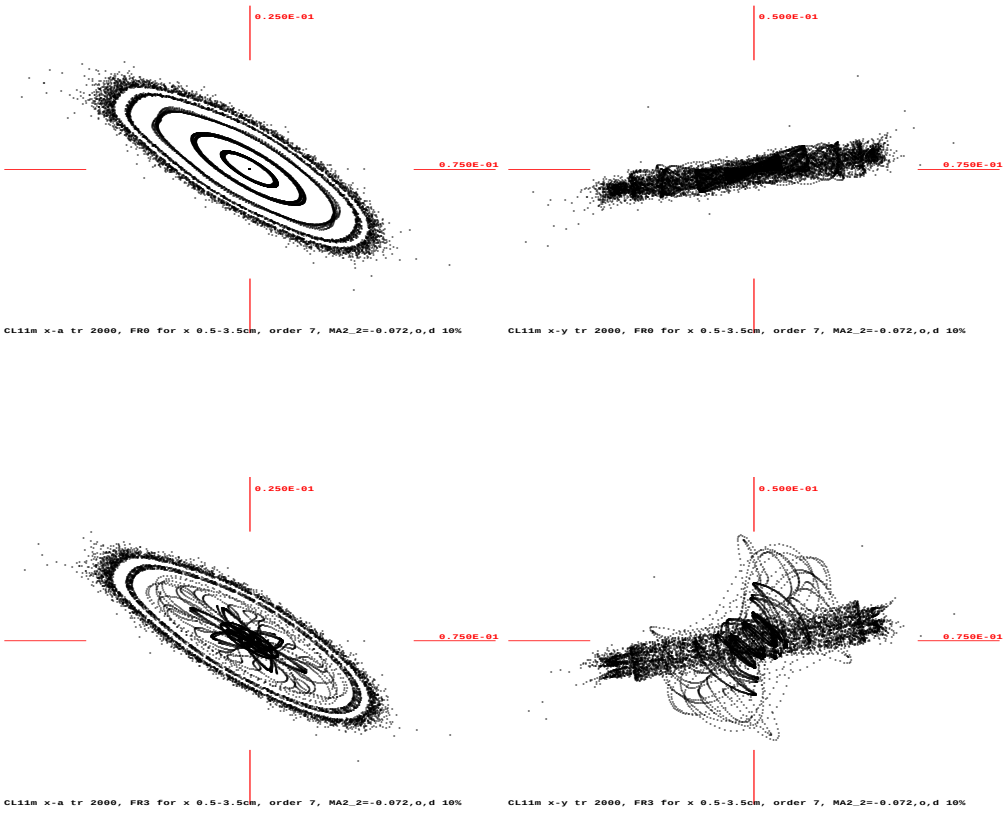

Fig. 9. Tracking with the additional multipole components, with the normal sextupole, skew octupole and normal decapole strengths 10% of the initial. Without/with (top/bottom) the fringe field consideration.

4 Preliminary 3D Simulations

As was noted, much more than a 2D multipole decomposition will be needed in order to assess the performance of this arc magnet configuration. When the analytical bar model is used for a 3D simulation, the first result is that this magnet configuration demonstrates a strong solenoidal component as mentioned before. The longitudinal field profile obtained from the s-dependence of the bar-magnet field in Figure 10 shows a surprisingly strong solenoidal field which peaks at 2.3 T on axis upon entering the single coil region. Such fields are not present in conventional magnets where midplane symmetry is preserved and cannot be described by a mere 2D analysis of normal or skew fields. These longitudinal fields manifest themselves only in the transition regions and change sign on entering and leaving the single-coil region – with much the same properties as the double-flip super-FOFO cooling channel. Since these fields are small outside the transition regions, they can be represented by a short solenoid, producing vertical and horizontal focusing over and above what is obtained through the quadrupole components in the combined-function region.

We studied the solenoidal effects by placing a solenoid with Gaussian shape

$$B(s) = B_0 \exp(-(s/D)^2)$$

at the double coil and the single coil transition regions with the maximum field strength B_0, 2.3T and the width D, 5cm, 10cm and 20cm in each study case. The tracking result is shown in Figures 11, 12 and 13, where the last set of higher multipole components is used, and the fringe field effects are studied as well. Without a full field map, all calculations are not verifiable as to the accuracy level. However, the magnitude of the effect should be indicative of the impact on the performance of the actual module. Both the slope of the solenoidal field profile and the integrated field seem to be important factors for the performance. If the magnet aperture is smaller, the maximum strength of the longitudinal field increases and the field profile becomes steeper. On the other hand, in general when the magnet aperture is small, the end field profile also is expected to be steeper, hence it might decrease the impact of the linear and lower order fringe field effects.

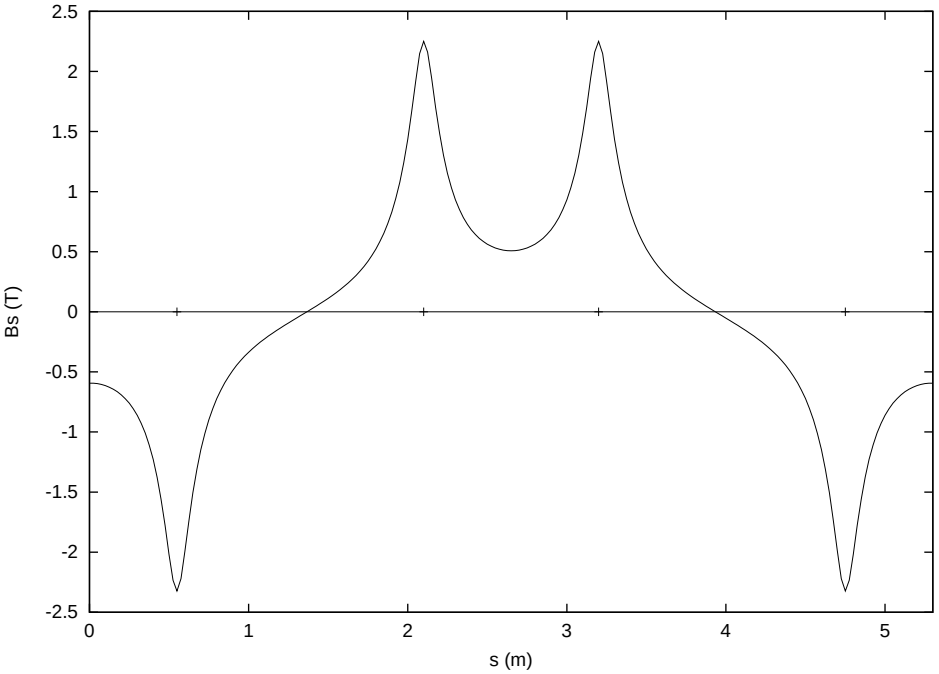

Fig. 10. Longitudinal field profile of the bar-magnet field.

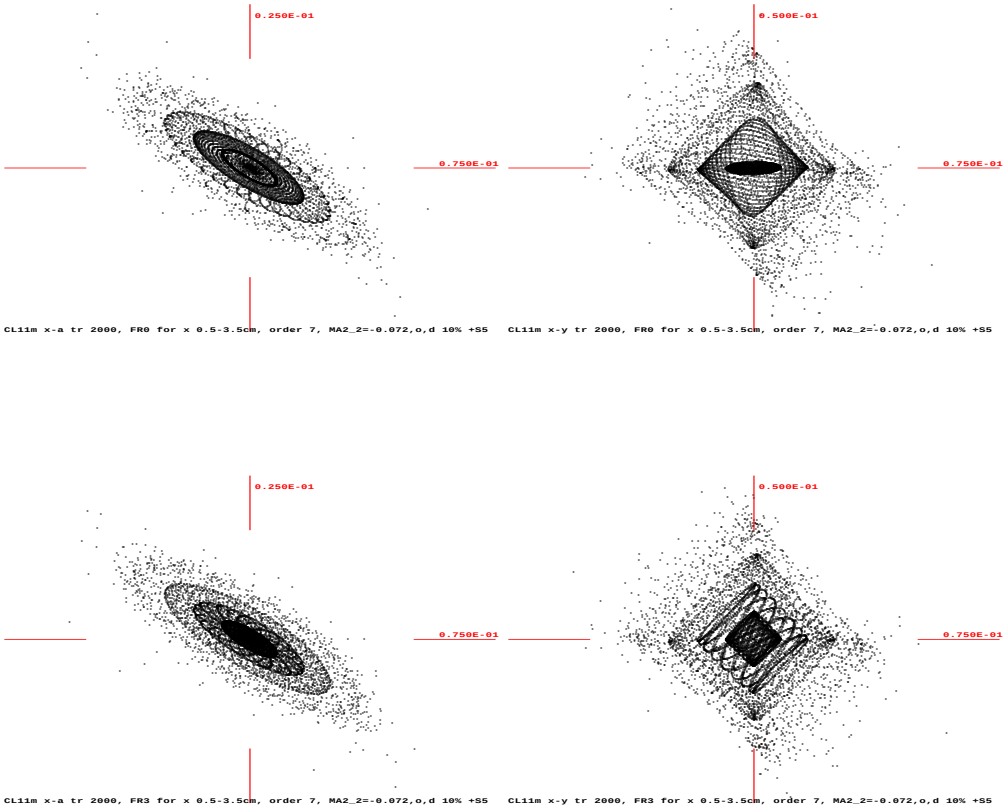

Fig. 11. Adding the solenoid components with $5cm$ Gaussian model to tracking with the additional multipole components, with the sextupole, octupole and decapole strengths 10% of the initial. Without/with (top/bottom) the fringe field consideration.

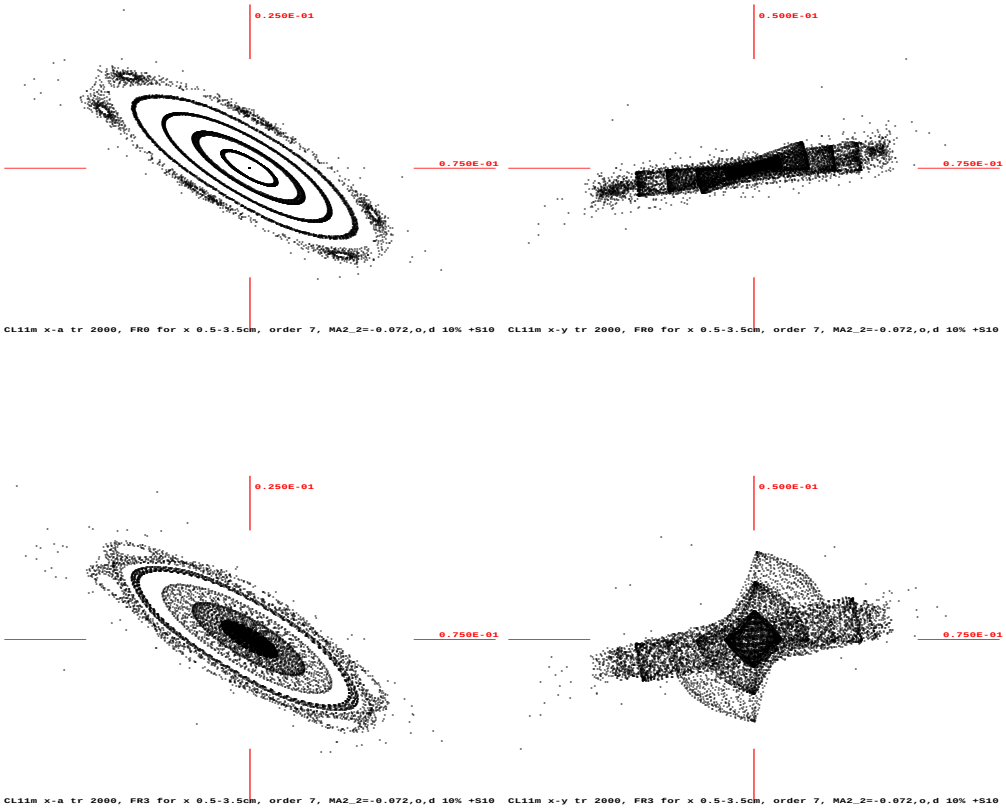

Fig. 12. Adding the solenoid components with $10cm$ Gaussian model.

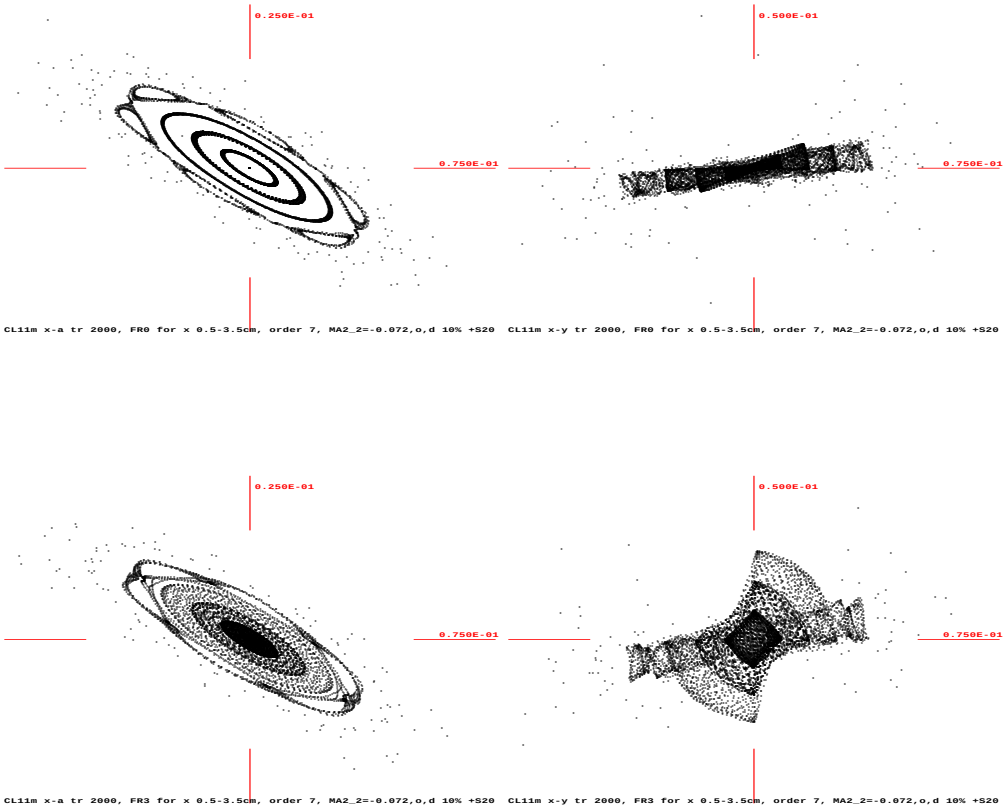

Fig. 13. Adding the solenoid components with 20cm Gaussian model.

5 Tunes

At last it is worthwhile to summarize the effects on the tunes for the cases studied above. In this report, only the linear tunes are reported. Table 5 lists the result.

Table 5
Linear tunes in each study case.

Figure	No Fringe Field Effects		With Fringe Field Effects
4. Thin lens model	x	0.1666670813217905	N/A
	y	0.1666670813217905	
4 - 9. Non-zero length model	x	0.1684223677184964	0.1680396455427017
	y	0.1684223677184963	0.1669187584941884
11. With additional solenoids	x	0.1810221175135072	0.1796152335940035
5cm Gaussian model	y	0.1810221174949308	0.1806592354141721
12. With additional solenoids	x	0.1748303967318750	0.1744582208706201
10cm Gaussian model	y	0.1748303967175597	0.1733778453610936
13. With additional solenoids	x	0.1716612350104970	0.1712839530234443
20cm Gaussian model	y	0.1716612350071255	0.1701838929148293

6 Conclusions and Recommendations for Further Work

The proposed design of a muon storage ring with longitudinal offset coils can have very clean linear optics with cylindrical symmetry. The study of nonlinear effects of the 60° arc cell indicates both the higher multipole components in the main body field of the magnets and the end fields have a large impact. Furthermore, it was found that there is very strong longitudinal field on axis, and the preliminary study indicates quite an impact by this solenoidal field component.

Overall, for the purposes of further analysis, it is strongly advised to perform a careful 3D analysis of the field profiles of the system. The following points appear particularly important.

1) Assure that as advertised, the reference orbit stays purely horizontal, and does not travel out of the midplane in the skew quadrupole region as a consequence of an initially horizontal displacement. This requires careful tracking of the reference particle as part of the initial magnet design. Furthermore, it seems advisable to provide for correction mechanisms like trim coils and possibly locations for iron shims (although the latter may prove less effective due to the high saturation) for correction of the reference orbit due to any unexpected field imperfections in the completed magnet.

2) Significantly reduce multipole components compared to R. Gupta's original design. Avoid additional multipole components in the end fields.

3) Determine the full longitudinal behavior of the Fourier modes in the field or its scalar potential for at least three suitable reference radii at a sufficient number of positions along the reference axis. Also determine higher order longitudinal derivatives of these Fourier modes, preferably by a method more sophisticated than numerical differentiation, but rather in agreement to the analytical expression.

4) Determine the on-axis solenoidal (zeroth order Fourier mode) field component as a function of longitudinal position

5) Perform additional simulations of the nonlinear dynamics, now including the nonlinearities introduced by the multipoles and their derivatives, as well as the additional linear focusing from the solenoidal field components.

References

[1] M. Berz. COSY INFINITY Version 8 reference manual. Technical Report MSUCL-1088, National Superconducting Cyclotron Laboratory, Michigan State University, East Lansing, MI 48824, 1997. see also http://cosy.nscl.msu.edu.

[2] B. Parker. Neutrino factory feasibility study ii, storage ring lattice magnetic design. http://magnets.rhic.bnl.gov/staff/parker/parker29jan01.pdf.

[3] M. Berz. *Modern Map Methods in Particle Beam Physics*. Academic Press, San Diego, 1999.

[4] M. M. Gordon and T. Taivassalo. The z^4 orbit code and the focusing bar fields used in beam extraction calculations for superconducting cyclotrons. *Nuclear Instruments and Methods*, 247:423, 1986.

[5] M. Berz, B. Erdelyi, and K. Makino. Fringe field effects in small rings of large acceptance. *Physical Review ST-AB*, 3:124001, 2000.

Appendix: Simulation Program coded in COSY Infinity

```
 1  INCLUDE 'COSY' ;
 2
 3  PROCEDURE RUN ;
 4   VARIABLE APER_BEND 1 ;
 5   VARIABLE MU 50 3 ; VARIABLE I 1 ; VARIABLE LFF 1 ; VARIABLE LSOL 1 ;
 6   VARIABLE MAPD0 1000 8 ; VARIABLE MAPD1 1000 8 ; VARIABLE MAPD2 1000 8 ;
 7   VARIABLE MAPQF 1000 8 ; VARIABLE MAPQD 1000 8 ;
 8   VARIABLE MAPSP 1000 8 ; VARIABLE MAPSM 1000 8 ;
 9   VARIABLE MA10 1 ; VARIABLE MA1 1 20 ; VARIABLE MA20 1 ; VARIABLE MA2 1 20 ;
10   VARIABLE MSF 1 20 ; VARIABLE MSD 1 20 ; VARIABLE NPM 1 ;
11   VARIABLE DSOL 1 ; VARIABLE TMP 1 ; VARIABLE STR 80 ;
12
13   PROCEDURE NGDR ; DL -1.55 ; ENDPROCEDURE ;
14   PROCEDURE NGDR10 ; DL -0.155 ; ENDPROCEDURE ;
15   PROCEDURE NGDR5 ; DL -0.11 ; ENDPROCEDURE ;
16
17   PROCEDURE D1H ;
18    VARIABLE NT 1 ; VARIABLE KN 1 2 ; VARIABLE S1 1 2 ; VARIABLE S2 1 2 ;
19    NT := 1 ; KN(1) := -0.5483113556171055E-02 ; S1(1) := 0 ; S2(1) := 0 ;
20    RA -45 ; MCLK  0.55 3.3000000000031 APER_BEND KN S1 S2 NT ;
21    RA 45 ; ENDPROCEDURE ;
22
23   PROCEDURE D1H5 ;
24    VARIABLE NT 1 ; VARIABLE KN 1 2 ; VARIABLE S1 1 2 ; VARIABLE S2 1 2 ;
25    NT := 1 ; KN(1) := -0.5483113556171055E-02 ; S1(1) := 0 ; S2(1) := 0 ;
26    RA -45 ; MCLK  0.11 0.66000000000062 APER_BEND KN S1 S2 NT ;
27    RA 45 ; ENDPROCEDURE ;
28   PROCEDURE MM1H5 ;
29    RA -45 ; MM 0.11 MA2 NPM APER_BEND ; RA 45 ; ENDPROCEDURE ;
30
31   PROCEDURE D2I ;
32    VARIABLE NT 1 ; VARIABLE KN 1 2 ; VARIABLE S1 1 2 ; VARIABLE S2 1 2 ;
33    NT := 1 ; KN(1) := -0.1370778389042764E-02 ; S1(1) := 0 ; S2(1) := 0 ;
34    RA -45 ; MCLK  1.55 4.650000000004368 APER_BEND KN S1 S2 NT ;
35    RA 45 ; ENDPROCEDURE ;
36   PROCEDURE D2I10 ;  {1/10 of D2I}
37    VARIABLE NT 1 ; VARIABLE KN 1 2 ; VARIABLE S1 1 2 ; VARIABLE S2 1 2 ;
38    NT := 1 ; KN(1) := -0.1370778389042764E-02 ; S1(1) := 0 ; S2(1) := 0 ;
39    RA -45 ; MCLK 0.155 0.4650000000004368 APER_BEND KN S1 S2 NT ;
40    RA 45 ; ENDPROCEDURE ;
41
42   PROCEDURE Q2DI ;
```

```
 VARIABLE NT 1 ; VARIABLE KN 1 2 ; VARIABLE S1 1 2 ; VARIABLE S2 1 2 ;
 NT := 2 ;
 KN(1) :=  0.3026937382542003E+00 ; KN(2) :=  0.6586774193548390E-02 ;
 S1(1) := 0 ; S1(2) := 0 ; S2(1) := 0 ; S2(2) := 0 ;
 MCLK 1.55 0 APER_BEND KN S1 S2 NT ; ENDPROCEDURE ;
PROCEDURE Q2DI10 ; {1/10 of Q2DI}
 VARIABLE NT 1 ; VARIABLE KN 1 2 ; VARIABLE S1 1 2 ; VARIABLE S2 1 2 ;
 NT := 2 ;
 KN(1) :=  0.3026937382542003E+00 ; KN(2) :=  0.6586774193548390E-02 ;
 S1(1) := 0 ; S1(2) := 0 ; S2(1) := 0 ; S2(2) := 0 ;
 MCLK 0.155 0 APER_BEND KN S1 S2 NT ; ENDPROCEDURE ;

PROCEDURE MMSD ;
 RA -45 ; MMS 0.155 MA1 MSD NPM APER_BEND ; RA 45 ; ENDPROCEDURE ;

PROCEDURE Q2FI ;
 VARIABLE NT 1 ; VARIABLE KN 1 2 ; VARIABLE S1 1 2 ; VARIABLE S2 1 2 ;
 NT := 2 ;
 KN(1) := -0.3026937382542003E+00 ; KN(2) := -0.9659354838709682E-02 ;
 S1(1) := 0 ; S1(2) := 0 ; S2(1) := 0 ; S2(2) := 0 ;
 MCLK 1.55 0 APER_BEND KN S1 S2 NT ; ENDPROCEDURE ;
PROCEDURE Q2FI10 ; {1/10 of Q2FI}
 VARIABLE NT 1 ; VARIABLE KN 1 2 ; VARIABLE S1 1 2 ; VARIABLE S2 1 2 ;
 NT := 2 ;
 KN(1) := -0.3026937382542003E+00 ; KN(2) := -0.9659354838709682E-02 ;
 S1(1) := 0 ; S1(2) := 0 ; S2(1) := 0 ; S2(2) := 0 ;
 MCLK 0.155 0 APER_BEND KN S1 S2 NT ; ENDPROCEDURE ;

PROCEDURE MMSF ;
 RA -45 ; MMS 0.155 MA1 MSF NPM APER_BEND ; RA 45 ; ENDPROCEDURE ;

   PROCEDURE CL11ver2 ; {Second thick lens version, Not quite right.}
    FR 0 ; D1H ;
    FR LFF ; Q2FI ; NGDR ; FR 0 ; D2I ;
    D1H ; D1H ;
    FR LFF ; Q2DI ; NGDR ; FR 0 ; D2I ;
    D1H ;
    ENDPROCEDURE ;

   PROCEDURE CL11ver3 ; {Third thick lens version}
    {D1H only exit ff}  FR 0 ; D1H ; IF LFF=3 ; FR -2 ; D1H ; ENDIF ;
    {Q2FI10 and D2I10 only ent  ff}
      IF LFF=3 ; FR -1 ; Q2FI10 ; D2I10 ; ENDIF ;
    {10 of Q2FI10 and D2I10 without ff} FR 0 ;
    LOOP I 1 10 ; Q2FI10 ; NGDR10 ; D2I10 ; ENDLOOP ;
```

```
 88       {Q2FI10 and D2I10 only exit ff}
 89         IF LFF=3 ; FR -2 ; Q2FI10 ; D2I10 ; ENDIF ;
 90       {D1H only ent  ff}  IF LFF=3 ; FR -1 ; D1H ; ENDIF ; FR 0 ; D1H ;
 91       {D1H only exit ff}  FR 0 ; D1H ; IF LFF=3 ; FR -2 ; D1H ; ENDIF ;
 92       {Q2DI10 and D2I10 only ent ff}
 93         IF LFF=3 ; FR -1 ; Q2DI10 ; D2I10 ; ENDIF ;
 94       {10 of Q2DI10 and D2I10 without ff} FR 0 ;
 95       LOOP I 1 10 ; Q2DI10 ; NGDR10 ; D2I10 ; ENDLOOP ;
 96       {Q2DI10 and D2I10 only exit ff}
 97         IF LFF=3 ; FR -2 ; Q2DI10 ; D2I10 ; ENDIF ;
 98       {D1H only ent  ff}  IF LFF=3 ; FR -1 ; D1H ; ENDIF ; FR 0 ; D1H ;
 99       ENDPROCEDURE ;
100
101      PROCEDURE CLMULS ; {With realistic multipole components and solenoids}
102       UM ; FR 0 ; D1H5 ; NGDR5 ; MM1H5 ; SM MAPD0 ;
103       IF LFF=3 ;
104          UM ; FR -1 ; D1H5 ; MM1H5 ; SM MAPD1 ;
105          UM ; FR -2 ; D1H5 ; MM1H5 ; SM MAPD2 ;
106          ENDIF ;
107       UM ; FR 0 ; Q2FI10 ; NGDR10 ; MMSF ; NGDR10 ; D2I10 ; SM MAPQF ;
108       UM ; FR 0 ; Q2DI10 ; NGDR10 ; MMSD ; NGDR10 ; D2I10 ; SM MAPQD ;
109       IF LSOL=1 ;
110          UM ; CMG  2.3 DSOL ; SM MAPSP ;
111          UM ; CMG -2.3 DSOL ; SM MAPSM ; ENDIF ;
112
113       UM ;
114       {5 of D1H5 without ff}
115       LOOP I 1 5 ; AM MAPD0 ; ENDLOOP ;
116       {D1H5 only exit ff}
117         IF LFF=3 ; AM MAPD2 ; ENDIF ;
118       {-Solenoid} IF LSOL=1 ; AM MAPSM ; ENDIF ;
119       {Q2FI10 and D2I10 only ent  ff}
120         IF LFF=3 ; FR -1 ; Q2FI10 ; MMSF ; D2I10 ; ENDIF ;
121       {10 of Q2FI10 and D2I10 without ff}
122       LOOP I 1 10 ; AM MAPQF ; ENDLOOP ;
123       {Q2FI10 and D2I10 only exit ff}
124         IF LFF=3 ; FR -2 ; Q2FI10 ; MMSF ; D2I10 ; ENDIF ;
125       {+Solenoid} IF LSOL=1 ; AM MAPSP ; ENDIF ;
126       {D1H5 only ent  ff}
127         IF LFF=3 ; AM MAPD1 ; ENDIF ;
128       {5 of D1H5 without ff}
129       LOOP I 1 5 ; AM MAPD0 ; ENDLOOP ;
130       {5 of D1H5 without ff}
131       LOOP I 1 5 ; AM MAPD0 ; ENDLOOP ;
132       {D1H5 only exit ff}
```

```
133         IF LFF=3 ; AM MAPD2 ; ENDIF ;
134       {+Solenoid} IF LSOL=1 ; AM MAPSP ; ENDIF ;
135       {Q2DI10 and D2I10 only ent ff}
136         IF LFF=3 ; FR -1 ; Q2DI10 ; MMSD ; D2I10 ; ENDIF ;
137       {10 of Q2DI10 and D2I10 without ff}
138       LOOP I 1 10 ; AM MAPQD ; ENDLOOP ;
139       {Q2DI10 and D2I10 only exit ff}
140         IF LFF=3 ; FR -2 ; Q2DI10 ; MMSD ; D2I10 ; ENDIF ;
141       {-Solenoid} IF LSOL=1 ; AM MAPSM ; ENDIF ;
142       {D1H5 only ent  ff}
143         IF LFF=3 ; AM MAPD1 ; ENDIF ;
144       {5 of D1H5 without ff}
145       LOOP I 1 5 ; AM MAPD0 ; ENDLOOP ;
146       ENDPROCEDURE ;
147
148      PROCEDURE MULTI FL ; {multipole components}
149       VARIABLE R0 1 ; VARIABLE FACT 1 ; FACT := 1 ;
150       LOOP I 1 20 ; MA2(I) := 0 ; MA1(I) := 0 ; MSF(I) := 0 ; ENDLOOP ;
151       IF FL<1.5 ; {Bela}
152          WRITE 8 ' Bela''s Multipole components in COSY notation' ;
153          MA20    :=  6.999999999999 ;
154          MA2(2)  := -0.419967202357 ;
155          MA2(4)  := -0.048058804186 ;
156          MA2(6)  := -0.002930967194 ;
157          MA2(8)  :=  0.000252539422 ;
158          MA2(10) :=  0.000101543927 ;
159          MA2(12) :=  0.000014073223 ;
160
161          MA10    :=  3.540958193499 ;
162          MA1(2)  := -0.209972229705 ;
163          MA1(4)  := -0.024029399698 ;
164          MA1(6)  := -0.001465483598 ;
165          MA1(8)  :=  0.000126269711 ;
166          MA1(10) :=  0.000050771963 ;
167          MA1(12) :=  0.000007036611 ;
168
169          MSF(1)  :=  1.184123248558 ;
170          MSF(3)  :=  0.020343804389 ;
171          MSF(5)  := -0.004653395920 ;
172          MSF(7)  := -0.001034945328 ;
173          MSF(9)  := -0.000102938909 ;
174          MSF(11) :=  0.000001434623 ;
175          MSF(13) :=  0.000002518965 ;
176
177          R0 := 0.065 ; NPM := 13 ;
```

```
178          IF FL=1 ; WRITE 8 ' with factoring' ;
179             LOOP I 1 NPM ; FACT := FACT*APER_BEND/R0 ;
180                MA2(I) := MA2(I)*FACT ; MA1(I) := MA1(I)*FACT ;
181                MSF(I) := MSF(I)*FACT ; ENDLOOP ; ENDIF ;
182       ELSEIF FL=2 ; {Ramesh}
183          WRITE 8 ' Ramesh''s Multipole components in COSY notation' ;
184          MA20    :=  6.34982 ;
185          MA2(2)  := -1.0763E-2*MA20 ;
186          MA2(4)  := -4.5972E-4*MA20 ;
187          MA2(6)  := -6.4354E-6*MA20 ;
188
189          MSF(3)  := -MA2(4) ;
190          MSF(5)  :=  0.1*MSF(3) ;
191          MSF(7)  := -0.1*MSF(5) ;
192
193          R0 := 0.02 ; NPM := 7 ;
194          LOOP I 1 NPM ; FACT := FACT*APER_BEND/R0 ;
195             MA2(I) := MA2(I)*FACT ; MA1(I) := 0.5*MA2(I) ;
196             MSF(I) := MSF(I)*FACT ; ENDLOOP ;
197       ENDIF ;
198
199       MSF(1) := 0 ;
200       LOOP I 1 20 ; MSD(I) := -MSF(I) ; ENDLOOP ;
201
202       WRITE 8 '         MA2                  MA1                  MSF' ;
203       LOOP I 1 NPM ;
204          WRITE 8 ( SF(I,'(I3)')&SF(MA2(I),'(E21.12)')&
205           SF(MA1(I),'(E21.12)')&SF(MSF(I),'(E21.12)') ) ; ENDLOOP ;
206       ENDPROCEDURE ;
207
208    APER_BEND := 0.065 ;
209
210    OV 7 2 0 ; RP 20000 0.1134289168 1 ; write 6 'CHIM is' CHIM ;
211
212    OPENF 8 'Multi.dat' 'UNKNOWN' ; MULTI 0 ; MULTI 2 ;
213
214   {Sextu, Oct, Deca setting}
215 {  TMP := 0          ; MA2(2) := TMP ; MA1(2) := 0.5*TMP ;}
216    TMP := 0.1*MA2(2) ; MA2(2) := TMP ; MA1(2) := 0.5*TMP ;
217    TMP := 0.1*MA2(4) ; MA2(4) := TMP ; MA1(4) := 0.5*TMP ;
218    TMP := 0.1*MSF(3) ; MSF(3) := TMP ; MSD(3) := -TMP ;
219
220 {  All additional multipoles 0}
221 {  LOOP I 1 20 ; MA2(I) := 0 ; MA1(I) := 0 ;
222       MSF(I) := 0 ; MSD(I) := 0 ; ENDLOOP ;}
```

```
223
224 {  LSOL := 0 ;}
225    LSOL := 1 ;
226
227    DSOL := 0.2 ;
228
229 {  STR := ', MA2_2='&SF(MA2(2),'(F6.3)')&', Ramesh''s' ;}
230 {  STR := ', MA2_2='&SF(MA2(2),'(F8.5)') ;}
231 {  STR := ', MA2_2='&SF(MA2(2),'(F8.5)')&' 10%' ;}
232 {  STR := ', MA2_2='&SF(MA2(2),'(F6.3)')&',o,d 10%' ;}
233    STR := ', MA2_2='&SF(MA2(2),'(F6.3)')&',o,d 10% +S20' ;
234
235    WRITE 8 ' *** Multipole components in use ***' ;
236    WRITE 8 ' *** '&STR ;
237    WRITE 8 '         MA2                  MA1                  MSF' ;
238    LOOP I 1 NPM ;
239       WRITE 8 ( SF(I,'(I3)')&SF(MA2(I),'(E21.12)')&
240        SF(MA1(I),'(E21.12)')&SF(MSF(I),'(E21.12)') ) ; ENDLOOP ;
241    CLOSEF 8 ;
242
243    LFF := 0 ; WRITE 6 ' CL11mul, FR '&SI(LFF) ;
244    UM ; CLMULS ; OPENF 9 'CLmF0.dat' 'UNKNOWN' ; write 9 ' *** '&STR ;
245    IF LSOL=1 ; write 9
246       ' *** Solenoid, Gaussian '&SF(DSOL*100,'(F4.1)')&'cm model' ; ENDIF ;
247    WRITE 9 ' BNL neutrino factory CL11mul, FR '&SI(LFF) ; PM 9 ;
248    WRITE 9 ' SE(MAP) = '&S(SE(MAP)) ; WRITE 6 ' tracking' ;
249    CR ; LOOP I 1 7 ; SR 0.005*I 0 0 0 0 0 0 0 1 ; ENDLOOP ;
250    TRT 'CL11m x-a tr 2000, FR0 for x 0.5-3.5cm, order '&SI(NO)&STR ;
251    TR 2000 1 1 2 0.075 0.025 0 0 -10 ;
252    TRT 'CL11m x-y tr 2000, FR0 for x 0.5-3.5cm, order '&SI(NO)&STR ;
253    TR 2000 1 1 3 0.075 0.05 0 0 -10 ;
254    WRITE 6 ' tunes' ; TS MU ;
255    WRITE 9 ' ORBITAL TUNES FROM TS:' MU(1) MU(2) ; CLOSEF 9 ;
256
257    LFF := 3 ; WRITE 6 ' CL11mul, FR '&SI(LFF) ;
258    UM ; CLMULS ; OPENF 9 'CLmF3.dat' 'UNKNOWN' ; write 9 ' *** '&STR ;
259    IF LSOL=1 ; write 9
260       ' *** Solenoid, Gaussian '&SF(DSOL*100,'(F4.1)')&'cm model' ; ENDIF ;
261    WRITE 9 ' BNL neutrino factory CL11mul, FR '&SI(LFF) ; PM 9 ;
262    WRITE 9 ' SE(MAP) = '&S(SE(MAP)) ; WRITE 6 ' tracking' ;
263    CR ; LOOP I 1 7 ; SR 0.005*I 0 0 0 0 0 0 0 1 ; ENDLOOP ;
264    TRT 'CL11m x-a tr 2000, FR3 for x 0.5-3.5cm, order '&SI(NO)&STR ;
265    TR 2000 1 1 2 0.075 0.025 0 0 -10 ;
266    TRT 'CL11m x-y tr 2000, FR3 for x 0.5-3.5cm, order '&SI(NO)&STR ;
267    TR 2000 1 1 3 0.075 0.05 0 0 -10 ;
```

```
268    WRITE 6 ' tunes' ; TS MU ;
269    WRITE 9 ' ORBITAL TUNES FROM TS:' MU(1) MU(2) ; CLOSEF 9 ;
270
271   ENDPROCEDURE ; RUN ; END ;
```